J Neurophysiol 114: 1424–1437, 2015.
First published June 3, 2015; doi:10.1152/jn.00980.2014.

A temperature rise reduces trial-to-trial variability of locust auditory neuron responses

Monika J. B. Eberhard,[1]* Jan-Hendrik Schleimer,[2,3]* Susanne Schreiber,[2,3] and Bernhard Ronacher[1,3]
[1]*Department of Biology, Behavioural Physiology Group, Humboldt-Universität zu Berlin, Berlin, Germany;* [2]*Department of Biology, Institute for Theoretical Biology, Humboldt-Universität zu Berlin, Berlin, Germany; and* [3]*Bernstein Center for Computational Neuroscience Berlin, Berlin, Germany*

Submitted 5 December 2014; accepted in final form 3 June 2015

Eberhard MJ, Schleimer JH, Schreiber S, Ronacher B. A temperature rise reduces trial-to-trial variability of locust auditory neuron responses. *J Neurophysiol* 114: 1424–1437, 2015. First published June 3, 2015; doi:10.1152/jn.00980.2014.—The neurophysiology of ectothermic animals, such as insects, is affected by environmental temperature, as their body temperature fluctuates with ambient conditions. Changes in temperature alter properties of neurons and, consequently, have an impact on the processing of information. Nevertheless, nervous system function is often maintained over a broad temperature range, exhibiting a surprising robustness to variations in temperature. A special problem arises for acoustically communicating insects, as in these animals mate recognition and mate localization typically rely on the decoding of fast amplitude modulations in calling and courtship songs. In the auditory periphery, however, temporal resolution is constrained by intrinsic neuronal noise. Such noise predominantly arises from the stochasticity of ion channel gating and potentially impairs the processing of sensory signals. On the basis of intracellular recordings of locust auditory neurons, we show that intrinsic neuronal variability on the level of spikes is reduced with increasing temperature. We use a detailed mathematical model including stochastic ion channel gating to shed light on the underlying biophysical mechanisms in auditory receptor neurons: because of a redistribution of channel-induced current noise toward higher frequencies and specifics of the temperature dependence of the membrane impedance, membrane potential noise is indeed reduced at higher temperatures. This finding holds under generic conditions and physiologically plausible assumptions on the temperature dependence of the channels' kinetics and peak conductances. We demonstrate that the identified mechanism also can explain the experimentally observed reduction of spike timing variability at higher temperatures.

temperature; grasshopper; auditory neuron; intrinsic variability

BECAUSE PHYSIOLOGICAL PROCESSES strongly depend on temperature, all aspects of animal life are affected by it. Chemical reaction rates typically exhibit Q_{10} values of 2.5–4 (Hoffmann 1995; Sanborn 2006), posing a challenge for ectothermic animals, such as insects, whose body temperatures are tightly coupled to the ambient temperature and whose body functions usually have to be maintained over a broad temperature range of $>20°C$. For the nervous system of these animals, in particular, variations in temperature modulate fundamental properties of neurons, resulting in changes of spike rates, conduction velocity, or transmitter release (Burrows 1989; Franz and Ronacher 2002; Janssen 1992; Montgomery and MacDonald 1990; Robertson and Money 2012). As a consequence, the processing of sensory information as well as the coordination of movements should be affected. Nevertheless, several aspects of nervous system function of ectothermic animals have been found to show a relatively high level of robustness to temperature changes (e.g. Caplan et al. 2014; Rinberg et al. 2013; Roemschied et al. 2014; Tang et al. 2010) despite various temperature-induced modifications in their elements—features that we are currently only beginning to understand.

In this study, we investigated the effect of temperature on sensory processing in the auditory periphery of locusts, with a focus on the variability of spiking responses. Earlier investigations on locust auditory receptors and interneurons revealed an improved temporal resolution at higher temperatures (Franz and Ronacher 2002; Prinz and Ronacher 2002; Ronacher and Römer 1985). The neurophysiological data were complemented by behavioral tests: females of the grasshopper *Chorthippus biguttulus* are able to detect gaps as small as 1–2 ms in male songs at 35°C, whereas at 23°C larger gaps are necessary to allow detection (Ronacher and Stumpner 1988; von Helversen 1972; von Helversen and von Helversen 1997). A better temporal resolution might be due to faster deterministic dynamics at higher temperatures, but a reduction in neuronal noise might also account for these findings. However, it is currently not known how intrinsic neuronal noise is affected by temperature changes in these animals.

In the case of auditory receptor neurons, i.e., the cells in the first layer of the feedforward network that constitutes the locust auditory periphery, the largest noise source is cell intrinsic (as these neurons do not receive synaptic inputs from other cells). It is not obvious whether intrinsic noise is reduced at higher temperatures. On the contrary, in view of larger peak conductances and shorter activation time constants of ion channels, one may even expect increased noise levels at higher temperatures. We hence intracellularly recorded the responses of identified neurons, exposing them to two different temperatures. Interestingly, trial-to-trial spike variability was consistently reduced at the higher temperature. To understand the mechanisms underlying this reduction of spike jitter at warmer temperatures, we followed a theoretical modeling approach: a detailed conductance-based model, including stochastic ion channels, was used to study the impact of temperature on spike rate and spike timing. Employing analytical techniques as well as model simulations, we demonstrate that, indeed, voltage fluctuations at warmer temperatures are diminished in the vicinity of the firing threshold and, consequently, spike timing jitter is lowered. These findings hold under generic conditions

* M. J. B. Eberhard and J.-H. Schleimer contributed equally to this work.

Address for reprint requests and other correspondence: M. J. B. Eberhard, General Zoology and Zoological Systematics, Zoological Institute and Museum, Ernst-Moritz-Arndt-Universität Greifswald, Anklamer Str. 20, 17489 Greifswald, Germany (e-mail: monika.eberhard@uni-greifswald.de).

and biophysically plausible assumptions on the temperature dependence of the channels' kinetics and peak conductances. The identified mechanism is likely to generalize beyond the locust receptor neurons.

MATERIALS AND METHODS

Experimental animals and electrophysiology. Experiments were performed on adult male and female *Locusta migratoria* L. obtained from a commercial supplier and held at room temperature (22–25°C). Head, legs, wings, and gut were removed, and the animals were fixed with wax ventral side down onto a Peltier element (3 × 1.5 cm), which was attached to a holder. The thorax was opened dorsally and the metathoracic ganglion subsequently stabilized on a NiCr platform. The whole thorax was filled with locust saline solution (Pearson and Robertson 1981). Auditory receptors and interneurons were recorded intracellularly in the frontal auditory neuropil of the metathoracic ganglion with glass microelectrodes (borosilicate, GC100F-10; Harvard Apparatus, Edenbridge, UK) filled with a 3–5% solution of Lucifer yellow in 0.5 M LiCl. All electrophysiological experiments were conducted in a Faraday cage lined with foam prisms to minimize echoes. Neuronal responses were amplified (BRAMP-01; npi electronic, Tamm, Germany) and recorded by a data-acquisition board (BNC-2090A; National Instruments, Austin, TX; sampling rate = 20 kHz).

The temperature of the preparation was controlled via the Peltier element connected to a 2-V battery. A digital thermometer (GMH 3210, Greisinger electronic, Regenstauf, Germany) connected to a NiCr-Ni thermoelement (GTF 300, type K, Greisinger electronic) was used to monitor and record temperature. The thermoelement was fixed between the Peltier element and the torso of the locust (underneath the ganglion), to prevent any disturbances of the neuronal recording. In most experiments, recordings were conducted first at 28–30°C and then the preparation was cooled down to 20–22°C and recordings were repeated for the same neuron at the low temperature. Temperature changes at the Peltier element were completed in ~1 min. When the low temperature of the Peltier element had been reached, we waited another 2 min before the second recording started. Tissue temperature at electrophysiological recording sites was derived from temperature measurements at the Peltier element and calibrated according to a calibration curve that had been created previously by measuring temperatures with three thermoelements: one at the Peltier element, one directly at the inner side of the tympanum, and one at the ganglion (see Eberhard et al. 2014; Roemschied et al. 2014). While in the majority of the measurements the preparations were cooled down, in four preparations the temperature change was reversed, starting with a low temperature; the direction of temperature change had no influence on measured Q_{10} values. After completion of the recordings Lucifer yellow was injected into the recorded cell by application of hyperpolarizing current. The thoracic ganglia were then removed, fixed in 4% paraformaldehyde, dehydrated, and cleared in methyl salicylate. Stained cells were identified under a fluorescent microscope according to their characteristic morphology and physiology (Römer and Marquart 1984; Stumpner and Ronacher 1991). Altogether, we recorded from 13 receptor neurons and 25 local and 24 ascending interneurons in 57 preparations (30 males, 27 females; in 5 preparations, 2 neurons were recorded). Parts of the data on receptor neurons have already been used in a different context in previous studies (Eberhard et al. 2014; Roemschied et al. 2014); to compare the temperature dependence of neurons of all three processing stages, we chose to reinvestigate these data. Among local interneuron types, two segmental, one bisegmental, and two different T neurons were recorded; among ascending neurons, seven different neuron types were recorded (see Table 1).

Stimulation. To obtain spike rate-intensity functions, we used acoustic broadband stimuli (100-ms duration, 1- to 40-kHz bandwidth) repeated five times each at eight intensities, rising from 32 to 88 dB SPL. Acoustic stimuli were stored digitally and delivered by a custom-made program (LabVIEW 7 Express; National Instruments). After a 100-kHz D/A conversion (BNC-2090A; National Instruments), the stimulus was routed through a computer-controlled attenuator (ATN-01M; npi electronic) and an audio amplifier (Pioneer stereo amplifier A-207R; Pioneer Electronics). Acoustic stimuli were unilaterally broadcast by speakers (D2905/970000; Scan-Speak, Videbæk, Denmark) located at ±90° relative to the longitudinal axis of the preparation, at a distance of 30 cm from the animal. To control for directional sensitivity of a recorded neuron, the sound stimulation was first played from the left and then the right side, or vice versa. Sound intensity was calibrated with a 0.5-in. microphone (type 4133; Brüel & Kjær, Nærum, Denmark) and a measuring amplifier (type 2209; Brüel & Kjær) positioned at the location of the preparation.

To test for changes in intrinsic variability for more complex stimuli, an additional set of stimuli was used in 15 recordings (see Fig. 5, Table 1, and Table 2): two model songs containing rectangular syllable envelopes, corresponding to mean syllable-pause lengths measured in *Ch. biguttulus* male songs at 30°C and 20°C (block1 and block2), part of a natural song recorded from a *Ch. biguttulus* male singing at 30°C (Origsong1), and the same natural song expanded 1.7 times to correspond to a natural song at 20°C according to von Helversen (1972) (Origsong2). All stimulus envelopes were filled with a broadband noise of 1- to 40-kHz bandwidth. Song stimuli were presented eight times each at 70 dB SPL, usually from the side (left or right) that showed a more sensitive reaction during presentation of

Table 1. *Temperature dependence of locust auditory neurons*

Neuron Type	Neuron Name	No. of Recordings	Model Songs Tested	Mean ± SD Q_{10}	Median Q_{10}
Receptors		13	2	1.38 ± 0.19	1.33
Local interneurons	SN1	6		1.81 ± 0.54	1.71
	SN4	1		2.40	2.40
	BSN1	11	2	3.14 ± 1.98	2.02
	TN1	6	2	1.69 ± 0.27	1.65
	TN4	1		3.24	3.24
Ascending interneurons	AN1	9	3	2.22 ± 1.20	1.74
	AN2	2	1	2.09 ± 1.10	2.09
	AN3	7	3	1.91 ± 0.76	1.72
	AN4	1	1	1.51	1.51
	AN11	2	1	1.74 ± 0.09	1.74
	AN12	2		1.30 ± 0.41	1.30
	AN15	1			

Values are numbers and names of recorded neurons together with mean ± SD and median Q_{10} for spike rate for each neuron type. For AN15 no Q_{10} (spike rate) could be calculated, as the neuron was inhibited for the duration of the stimulus. Each neuron was recorded at 2 different temperatures. Nomenclature after Römer and Marquart (1984) and Stumpner and Ronacher (1991).

Table 2. *Model songs used in electrophysiological recordings*

Model Song	No. of Syllables	Syllable Length, ms	Pause Length, ms	Total Length, ms
Block1	8	77	17	752
Block2	6	110	24	804
Origsong1	12	71.1	17.8	1020
Origsong2	12	121.9	30.2	1700

Note that for the original songs, mean syllable and pause lengths are given. See also Fig. 5.

the 100-ms stimuli. Note that locusts do not use calling songs for mate attraction; nevertheless, physiology and morphology of the auditory peripheral neurons are highly evolutionarily conserved and homologous for *L. migratoria* and *Ch. biguttulus* (Neuhofer et al. 2008).

Data analysis. Spike times were extracted from the digitized recordings by applying a voltage threshold. Mean spike rates were calculated to obtain spike rate-intensity functions per neuron, stimulation side, and temperature. From these curves, temperature coefficients (Q_{10} values) of the firing rate were determined. Rate changes with a 10° temperature shift can be expressed by the temperature coefficient Q_{10}:

$$Q_{10} = \left(\frac{X}{Y}\right)^{\frac{10}{\langle Tx-Ty \rangle}}$$

where X is the rate at higher temperature (Tx) and Y is the rate at the lower temperature (Ty). A mean Q_{10} value was subsequently calculated for each neuron using only values at intensities eliciting spike rates above a threshold set at 50% of the maximum spike rate at the high temperature (see Fig. 1*A*). In addition, Q_{10}s for first spike latencies as well as action potential duration (width) and amplitude (height) were calculated for each recorded neuron. To determine Q_{10}s for action potential width and height, spontaneous action potentials recorded during trials (before the start of a stimulus) were detected and superimposed and the mean action potential shape was calculated. From this, height and width at half of the action potential amplitude were measured for each neuron and temperature (see Fig. 2*D*). Significance of differences between high and low temperature for the various characteristics measured was estimated with Wilcoxon matched-pairs signed-rank tests, significance of differences in Q_{10} values of the three processing stages was calculated with Kruskal-Wallis tests, and post hoc pairwise comparisons were performed with Wilcoxon rank sum tests, Bonferroni corrected.

To estimate intrinsic variability (trial-to-trial variability) of spike responses for each neuron and temperature, the pairwise metric distance between spike trains of the five repetitions per stimulus intensity (or between the 8 repetitions of the model songs) was calculated according to van Rossum (2001). This metric yields an intuitive measure for the dissimilarity of spike trains, with large distance values indicating a high dissimilarity, that is, a large trial-to-trial variability. The van Rossum metric allows one to vary the temporal resolution of the comparison (via a resolution parameter τ). Equipped with very large τ values (>200 ms), the metric largely ignores differences in the timing of spikes, and spike train dissimilarity depends only on spike count differences. With τ values of a few milliseconds, differences between the spike trains in both spike count and spike timing contribute to the dissimilarity.

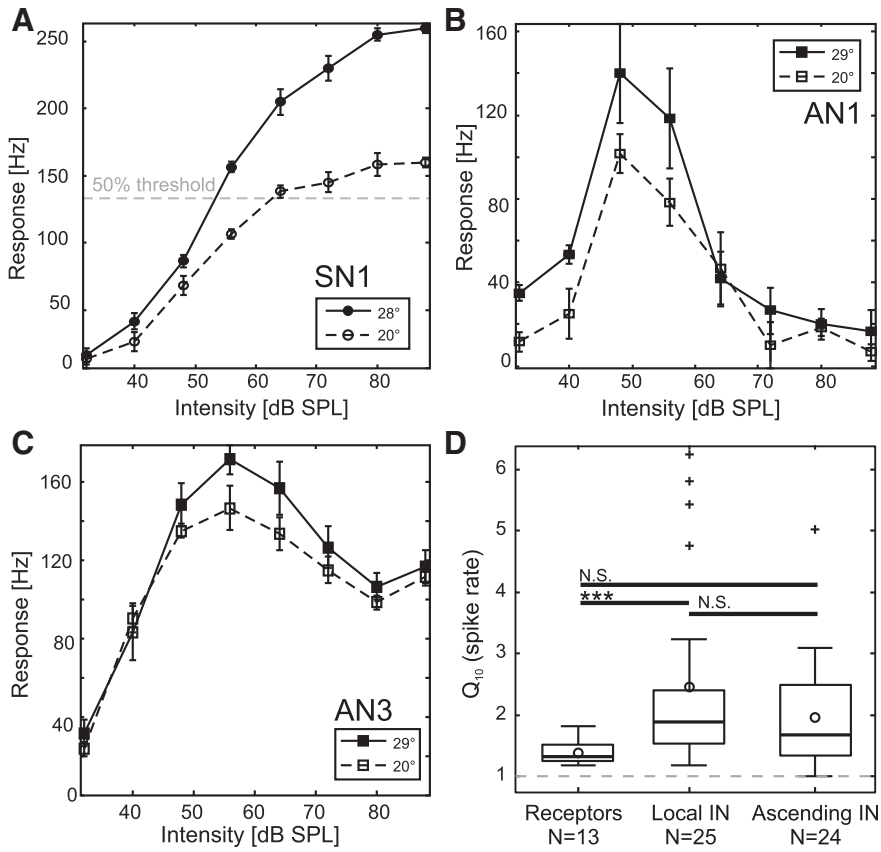

Fig. 1. Examples of spike rate-intensity functions obtained from locust auditory neurons at two different temperatures. *A*: local interneuron SN1. *B*: ascending interneuron AN1. *C*: ascending interneuron AN3 (for spike rate-intensity functions of receptor neurons see Eberhard et al. 2014; Roemschied et al. 2014). *D*: box plots of Q_{10} values of spike rate of all recorded cells showing means (circles), medians (thick lines), 25th/75th percentiles (boxes), 1.5 interquartile range (whiskers), and outliers (+); horizontal bars show pairwise comparisons (Wilcoxon signed-rank tests, Bonferroni corrected). ***$P < 0.001$. NS, not significant.

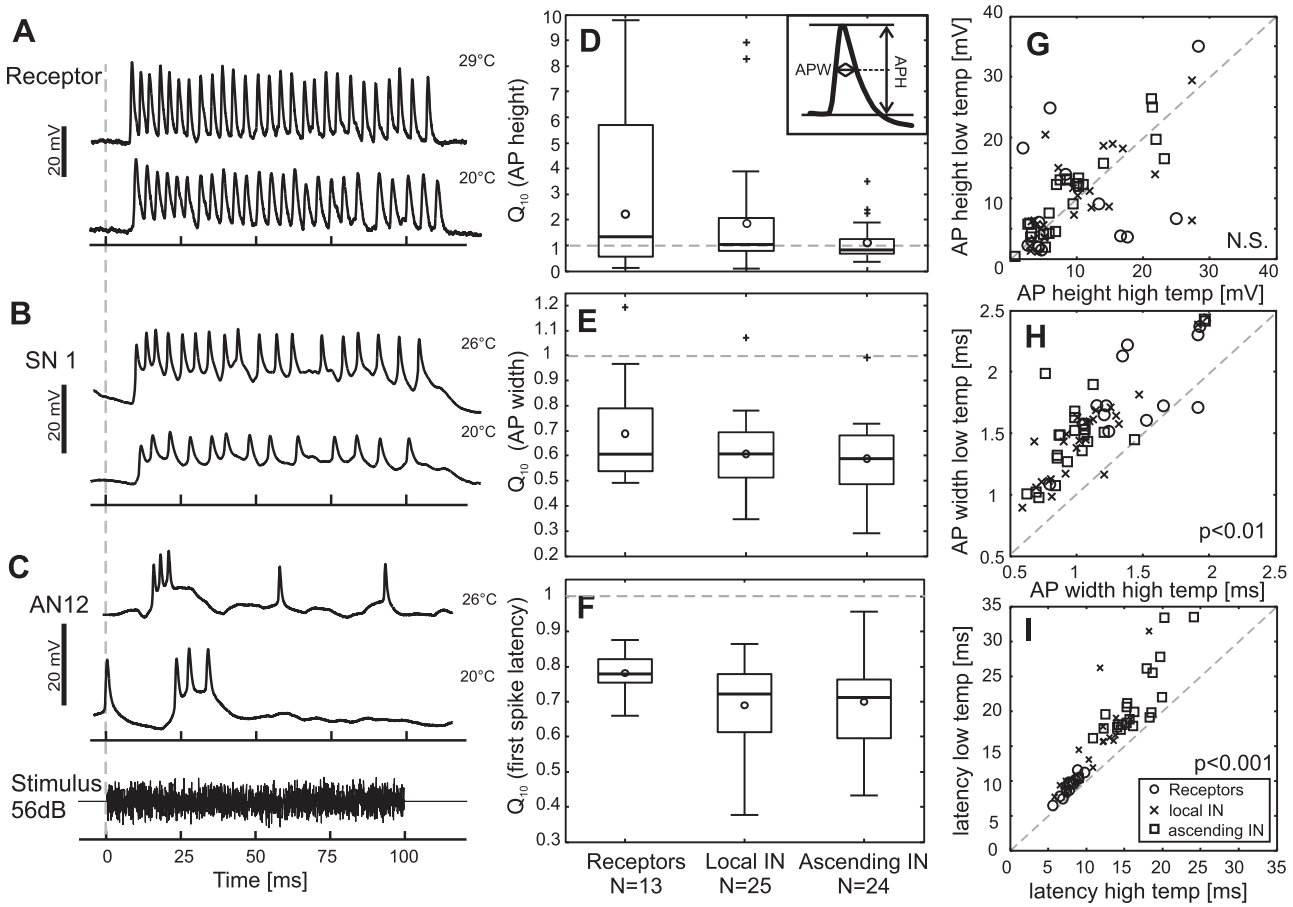

Fig. 2. Effect of temperature on characteristics of auditory neurons. *A–C*: voltage traces of a receptor (*A*) and a local (*B*) and an ascending (*C*) interneuron at high and low temperatures in response to a 100-ms auditory stimulus (56 dB SPL). *D–F*: box plots of Q_{10} values for action potential (AP) height (*D*), width (*E*), and first spike latency (*F*). *G–I*: pairwise comparisons of action potential height (*G*), width (*H*), and latency (*I*) at the 2 temperatures (hot and cold). *P* values shown were calculated with a Wilcoxon-matched pairs signed-rank test for each group.

Previous investigations showed that the timing of spikes plays an important role for the encoding of acoustic signals at the level of thoracic neurons (Franz and Ronacher 2002; Stumpner et al. 1991). Therefore we used a temporal resolution of $\tau = 5$ ms, which has been found to sufficiently encompass the coding properties of auditory neurons at different processing stages (Machens et al. 2003; Neuhofer et al. 2008; Wohlgemuth and Ronacher 2007). In addition, we also performed an analysis with τ varying between 2 and 1,024 ms.

The van Rossum distance also depends on the number of spikes (Neuhofer et al. 2011). To compare distance values between hot and cold recordings, which may differ in spike rates, we standardized the distance values by the square root of the number of spikes elicited during the stimulus, to get a comparable average distance (see APPENDIX A). Subsequently, one mean distance value per neuron was calculated (a mean distance over all intensities where a spike response was elicited and a mean distance per neuron for all model songs together, respectively). For the model songs, the first 150 ms of each recording were omitted, to analyze the responses in the adapted state only.

All analyses were done with MATLAB (R2012a, The MathWorks); graphs were edited in CorelDRAW (X6, Corel).

Simulation. The modeling approach was focused on the first processing stage, the receptor neurons. A model capturing mechanotransduction as well as spike generation was implemented. It had previously been fitted to the locust mechanoreceptors (Fisch et al. 2012) and replicates experimentally measured interspike interval distributions and serial correlations. For the transduction step, sound pressure waves evoke tympanal vibrations that in turn open and close mechanosensitive ion channels (APPENDIX B, *Eq. 7*). The parameters of the tympanal oscillator are based on experiments using laser vibrometry (Schiolten et al. 1981). Biophysical details of the model are described in APPENDIX B (see Fig. 6*A* for an equivalent circuit). All model parameters were taken from Fisch et al. (2012) and can be found in Table 4. Only the transduction parameters x_{base}, α, and k_s were adapted to fit our measured rate intensity curves. The temperature coefficients were chosen from realistic ranges (Hille 2001): Q_{10} values of the peak conductances ranged in the interval [1,2], while the Q_{10} values of the ion channel kinetics are between [2.5,4]. The exact values were chosen such that the temperature effect on the firing rate was comparable to that of the measured responses (see Fig. 6*B*).

The model was simulated at 22°C and 32°C. For the stimuli, $s(t) = 20 \times 10^{I_{\text{db}}(t)/20}\xi_s(t)$, the broadband carrier that is typical for grasshopper songs was described by a Gaussian white noise process $\xi_s(t)$. Two classes of stimuli were applied: *1*) a white noise carrier with constant amplitude $I_{\text{db}}(t) = \text{const.}$ given in dB SPL, to determine the rate-intensity curves (the result can be seen in Fig. 6*B*), and *2*) the same time-dependent amplitude modulation, $I_{\text{db}}(t)$, as in the natural songs used in experiments (Fig. 6*C*). Stochastic ion channels were approximated by a diffusion equation instead of simulating the channel's Markov models (Linaro et al. 2011). More details can be found in APPENDIX B. The simulated spike trains were analyzed in the same way as the experimentally recorded ones. All simulations were performed in the brian2 library (Stimberg et al. 2014). The temperature-compensated response in the firing rate

was achieved by selecting the Q_{10} values with a genetic algorithm (GA) from their given ranges. The GA objective was to minimize the mean squared difference between hot and cold response but was only allowed to choose realistic Q_{10} values from their respective intervals. For this the deap toolbox (Fortin et al. 2012), written in python, was used.

Analysis. To support the simulations and deepen the insight into the temperature effects on neuronal noise, formulas for the statistics of current and voltage fluctuations are provided in the following. Their detailed derivations can be found in APPENDIX C. In particular, the dependence on the temperature susceptibilities, Q_{10} values, is highlighted in the analysis. Peak conductances, ion channel kinetics, and reversal potentials depend on temperature, T in Kelvin, as follows:

$$\begin{aligned} g_k(T) &= g_k(T_{base})Q_{10}(g_k)^{(T-T_{base})/10}, \\ \tilde{\tau}_{ki}(T) &= \tilde{\tau}_{ki}(T_{base})Q_{10}(\tilde{\tau}_i)^{-(T-T_{base})/10}, \\ E_k(T) &= E_k(T_{base})\frac{T}{T_{base}} \end{aligned} \quad (1)$$

Here, the index k stands for elements of the set, $k \in K$, of all channel types. In our model these were $K = \{Na,K,M,R,L\}$ (see Fig. 6*A*). The time constants $\tilde{\tau}_{ki}$, together with the steady-state activation curves, which are not temperature dependent, describe the gating kinetics of channel k. Depending on the complexity of the underlying Markov model, there may be several time constants per channel involved.

To obtain a concise description of the total membrane current fluctuations in the receptor neuron model, it is approximated by a

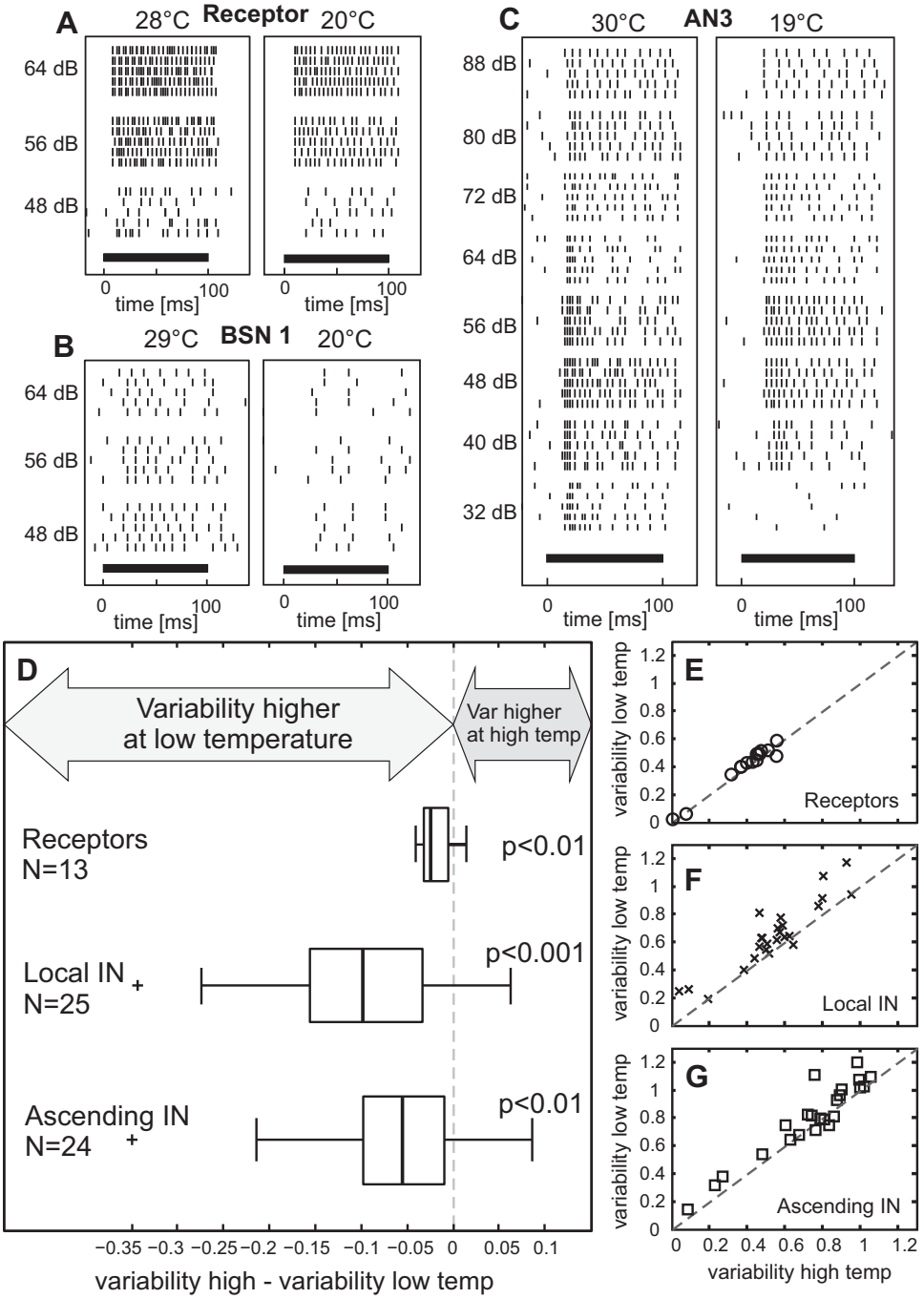

Fig. 3. *A–C*: spike-raster plots of example neurons recorded at high and low temperatures with short broadband noise stimuli at different intensities (indicated at the sides of the raster plots, dB SPL). Five repetitions per stimulus intensity are shown for a receptor neuron (*A*), local interneuron BSN1 (*B*) and ascending interneuron AN3 (*C*). *D*: variability values (metric distance in arbitrary units) calculated with the metric according to van Rossum, $\tau = 5$ ms: variability values at hot temperature minus those at cold temperature and *P* values from Wilcoxon matched-pairs signed-rank tests for all recorded neurons of the 3 processing stages. *E–G*: pairwise comparisons of distance values at hot vs. cold temperature for receptors (*E*) and local (*F*) and ascending (*G*) interneurons.

single colored, Gaussian noise process $\breve{\eta}$, with correlation function $\mathrm{cov}(\Delta) = \breve{\sigma}^2(v,T)e^{-\|\Delta\|/\breve{\tau}(v,T)}$. For a clamped voltage v and a fixed temperature T, the total noise power (i.e., the integral over the noise spectrum) is given by (cf. APPENDIX C)

$$\breve{\sigma}^2(v,T) = \sum_{k\in K}\sum_{i=1}^{M_k-1} \sigma_{ki}^2(v)g_k^2(T)\left(E_k(T)-v\right)^2 \quad (2)$$

The number of states in the channel's Markov model is denoted by M_k. The noise variance σ_{ki} associated with each channel state is defined in Linaro et al. (2011) and depends only on the steady-state activation curves, and hence not on temperature. With this approximation the temperature influences the total noise power only through the temperature susceptibilities of the peak conductances, $g_k(T)$, and the reversal potentials, $E_k(T)$. The effect on the reversal potentials is not substantial (~3%). The $Q_{10}(g_k)$ values are similar to that of aquatic diffusion and hence small compared with those of the reaction rates. In total, $\breve{\sigma}$ has a weak temperature dependence. In contrast, the time constant of the equivalent noise process $\breve{\eta}$, is given by

$$\breve{\tau}(v,T) = \frac{\breve{\sigma}^2(v,T)}{\sum_{k\in K}\sum_{i=1}^{M_k-1} g_k^2(T)\left(E_k(T)-v\right)^2\sigma_{ki}^2(v)/\tau_{ki}(v,T)} \quad (3)$$

only in some cases, like a simple two-state channel or the linear chain in the model's K^+ channel, $_{ki} \propto \tilde{\tau}_{ki}$; otherwise the expressions for the τ_{ki}s may involve several of the original $\tilde{\tau}_{ki}$s (cf. Linaro et al. 2011, Table 2). In general, the temperature scaling of $\breve{\tau}$ involves all Q_{10} values, including the strong temperature dependencies of the reaction kinetics. With this, the spectrum of the total noise current at a clamped command voltage v is then approximately a Lorentzian

$$P_I(f) = \frac{\breve{\tau}(v,T)\breve{\sigma}^2(v,T)}{1+\left(f\breve{\tau}(v,T)\right)^2} \quad (4)$$

The quantitative link between spike jitter and subthreshold membrane voltage fluctuations is nontrivial (Alijani and Richardson 2011), yet voltage noise is a better predictor than unfiltered current fluctuations. Therefore, the current spectrum in *Eq. 4* should be filtered by the membrane impedance to obtain the voltage fluctuations

$$\sigma_V^2 = \int \mathrm{d}f\, Z(f)P_I(f) \quad (5)$$

The impedance for our model can be approximated by (cf. APPENDIX C for a justification)

$$Z(f) \approx \frac{1}{\frac{1}{c}\left(\frac{\partial I_f}{\partial v}\right)^2 + f^2} \quad (6)$$

Note that the steady-state value of $\partial I_f/\partial v$, again, only depends on the Q_{10} parameters of the peak conductances, $g_c(T)$, and the reversal potentials, $E_c(T)$. Consequently, the impedance is affected by temperature to a lesser degree, as can be inspected in Fig. 7*B*.

RESULTS

The first three processing stages of the auditory pathway form a hierarchically organized feedforward network (in the metathoracic ganglion) and comprise receptor neurons, thoracic local interneurons, and ascending interneurons, respectively (Clemens et al. 2012; Stumpner et al. 1991; Stumpner and Ronacher 1991; Vogel and Ronacher 2007). First, we characterized effects of temperature on response characteristics of neurons across all three layers. To this end, each cell was recorded at two different temperatures (at approximately 20°C and 30°C).

Temperature effects on basic parameters of neuronal responses. In all 62 recorded neurons spike rate increased with higher temperature (Fig. 1, Table 1). The general shape of the spike rate-intensity functions did not change with temperature (i.e., saturating or unimodal curve; Fig. 1), nor was the basic spiking pattern of cells (phasic vs. tonic response) affected. On average, the temperature dependence of the spike rate was smallest in receptor neurons (mean Q_{10} of 1.38 ± 0.19, median: 1.33). For local and ascending interneurons the temperature effect was more pronounced [Fig. 1*D*; mean: 2.45 ± 1.48 (median: 1.88) and 1.96 ± 0.91 (median: 1.68), respectively; see also Table 1].

Temperature changes affected action potential shape and first spike latencies (Fig. 2). At all three processing stages, neurons exhibited a significant decrease in action potential width (Fig. 2, *E* and *H*) and latency (Fig. 2, *F* and *I*) with increased temperature, whereas spike amplitudes showed no consistent changes (Fig. 2, *D* and *G*). Q_{10} values for action potential height and width did not significantly differ between neurons at the three processing stages (Kruskal-Wallis test, AP height: $\chi^2 = 2.33$, $P = 0.31$, AP width: $\chi^2 = 1.31$, $P = 0.52$).

Temperature effects on intrinsic neuronal variability. Timing of spikes is thought to contribute to the neuronal represen-

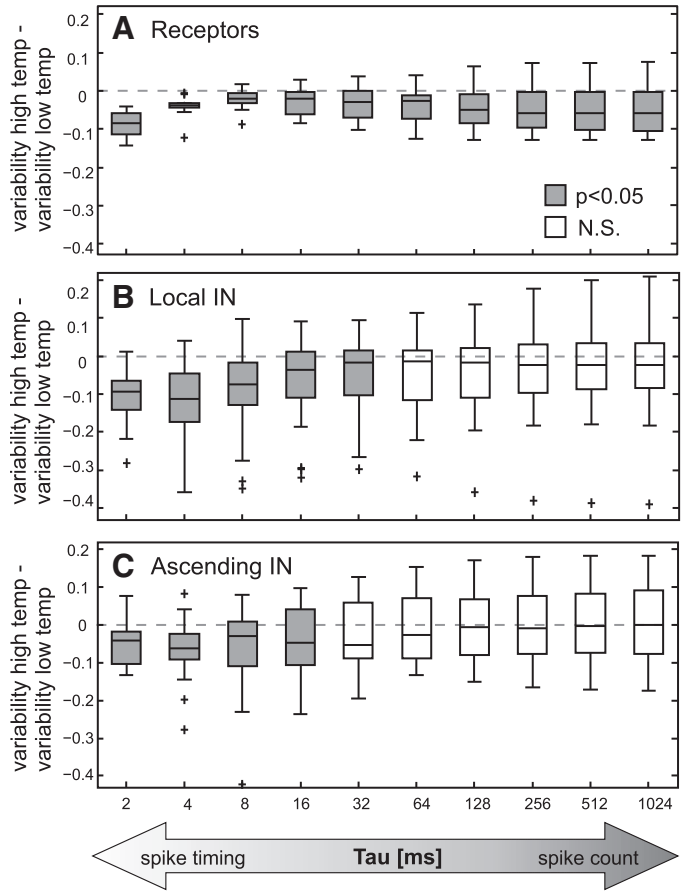

Fig. 4. Variability values at cold temperature subtracted from variability values at hot temperature for receptors (*A*) and local (*B*) and ascending (*C*) interneurons for different values of the metric's temporal resolution parameter τ. At large τ values only spike count differences contribute to the metric value, while for small τ differences in spike timing also become relevant. Gray box plots show a significant difference from zero (i.e., a significant change of intrinsic variability with temperature), while white boxes are not significantly different from zero (i.e., no change of variability with temperature).

tation of fast amplitude modulations in grasshopper acoustic communication signals (Machens et al. 2001; Wohlgemuth et al. 2011). Trial-to-trial variability of spiking responses can hence impair the processing of these vital signals.

We therefore quantified the trial-to-trial variability of responses, using the spike train metric introduced by van Rossum (2001). The metric can be applied with different values of the time constant τ (which is a parameter to the metric), setting the timescale of spike train comparison (small τ emphasizing spike timing on short timescales, large τ shifting emphasis rather to spike count than spike timing). Across cells from all processing stages of the peripheral network, spike train distances were significantly larger at the lower temperature, provided we used a high temporal resolution (τ = 5 ms; Fig. 3, Wilcoxon matched-pairs signed-rank tests). In other words, for both the short 100-ms acoustic stimuli (Fig. 3) and the longer model songs (see Fig. 5, *A–C*) spike timing variability was decreased at the warmer temperature.

For receptor neurons, in particular, this relation was observed across all values of τ used in the analysis (Fig. 4*A*). Hence, the intrinsic variability of spike count as well as of spike timing was decreased at warmer temperatures. For low values of τ, local and ascending interneurons exhibited the same trend, i.e., the spike timing variability decreased at higher temperature (Fig. 4, *B* and *C*). However, with larger τ values (>32 ms) differences in variability between the cold and warm temperatures disappeared, indicating that at these processing stages spike count variability was less affected by a temperature change than spike timing variability.

These results are further supported by the data obtained with long song models (Fig. 5). With a focus on spike timing, with a τ = 5 ms, most neurons exhibited a larger intrinsic variability

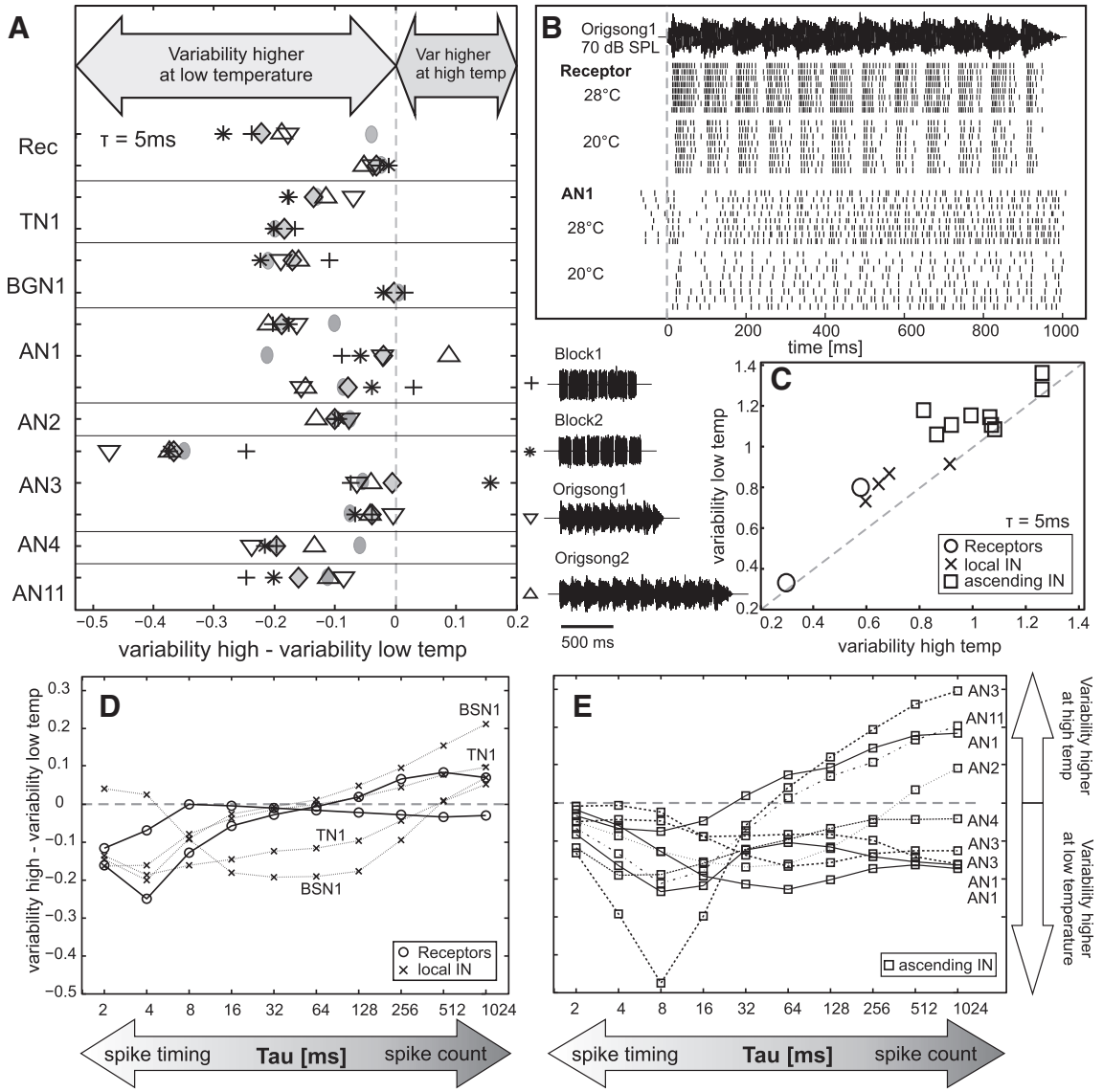

Fig. 5. Variability values resulting from applying the van Rossum metric to spike trains of neurons recorded during stimulation with the 4 model songs. *A*: variability values at hot temperatures minus values at cold temperatures for τ = 5 ms. Gray diamonds mark the mean variability calculated over all 4 model songs; gray circles indicate mean variability differences obtained with the short 100-ms stimuli. *B*: example spike-raster plots of a receptor neuron and ascending interneuron AN1, recorded at high and low temperatures; shown are 8 repetitions of the same stimulus (Origsong1). *C*: pairwise comparisons of mean variability values for τ = 5 ms. *D* and *E*: mean change (variability hot − variability cold) of intrinsic variability with temperature, using different values of τ. For each neuron, an average variability value for all 4 model songs was calculated.

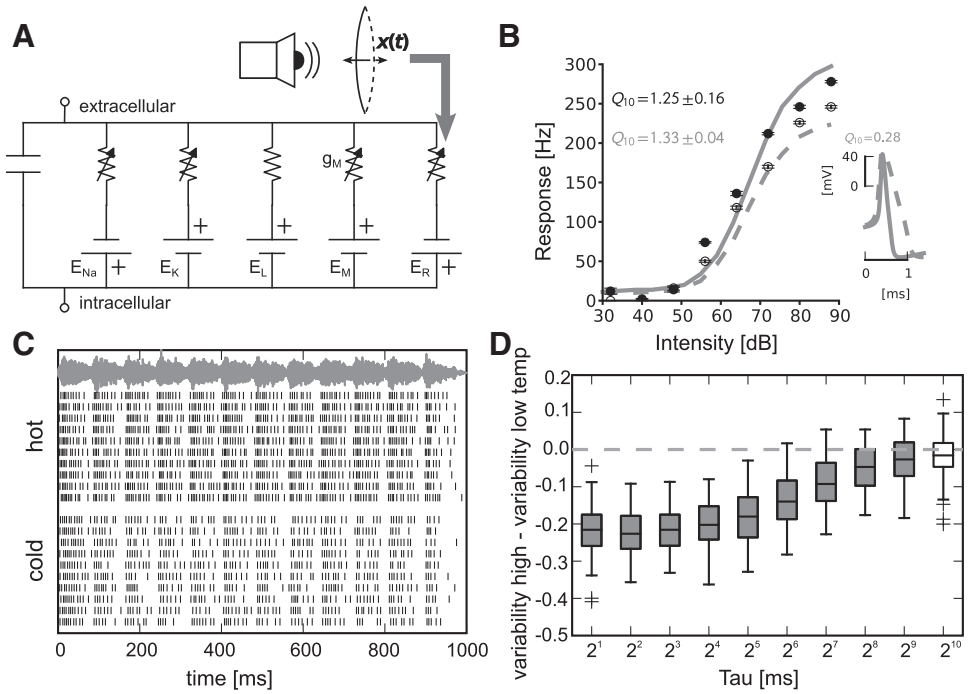

Fig. 6. *A*: equivalent circuit of the auditory receptor model. Tympanal vibrations are transduced by receptor channels (E_R). Other channels included in the model are spike-generating Na and K channels, leak channels (L), as well as adaptation channels (M). *B*: rate-intensity curves of the model at 22°C and 32°C. Also included in *B* is a plot of action potential width at 2 temperatures as derived from the model. *C*: spike response for natural, time-dependent stimuli at 22°C (cold) and 32°C (hot). *D*: average difference in spike train metric (hot − cold) for different values of τ. In all cases the distance value decreased at the high temperature, indicating both a decrease in spike-time jitter and spike count variability. Model and simulation parameters can be found in APPENDIX B.

at the lower temperature (Fig. 5, *A* and *C*). Similar as for the short acoustic stimuli, for small values of τ spike timing variability was on average larger at the low temperature whereas this effect disappeared or even reversed for larger τ values (Fig. 5, *D* and *E*).

Modeling. To identify the mechanisms underlying the observed reduction in intrinsic variability at elevated temperatures, we turned to computational modeling. Temperature is known to increase the peak conductances of ion channels. One may hence surmise a rise in conductance noise and, consequently, in current noise. Yet, two additional factors come into play: transition rates between channel states are also expedited, and the translation of current changes into voltage is governed by the membrane impedance, whose temperature dependence is likely to further modify the temperature effect on voltage noise. To dissect the impact of temperature on noise fluctuations at the different levels of current noise, voltage noise, and spike timing jitter, we analyzed a previously published quantitative model of the receptor dynamics (Fig. 6*A*).

First, a temperature dependence was introduced to this model assuming Q_{10} values for peak conductances and reaction rates of the individual ion channels (see *Eq. 1*) (Table 3). Q_{10} parameters were chosen from realistic parameter ranges to obtain rate-intensity curves with a temperature dependence comparable to that observed in the experimental data (Fig. 6*B*). For details on the chosen parameter set see APPENDIX B. Next, model responses to natural song stimuli were obtained from simulations at two different temperatures (Fig. 6*C*). The analysis of spike variability in the model yielded the same relation as in the experimental recordings: spike train variability was reduced at the warmer temperature (compare Fig. 6*D* and Fig. 4*A*).

Table 3. *Q_{10} parameters of peak conductances and activation and inactivation kinetics*

Parameter	Q_{10}	Parameter	Q_{10}
g_{Na}	2.00	Na act.	2.50
g_K	1.10	Na inact.	2.50
g_M	2.00	K act.	2.50
g_R	1.10	M act.	3.74
g_L	1.10	R act.	2.50

An advantage of this approach is that the model allows for an explicit dissection of the underlying biophysical mechanisms, which we discuss in the following. For moderate firing rates, spike jitter depends on voltage fluctuations at threshold (Alijani and Richardson 2011). The reduction in spike jitter should, therefore, be accompanied by smaller voltage fluctuations at the warmer temperature. To understand how the current noise produced by the multitude of stochastic ion channels affects voltage fluctuations, the model's noise current spectrum and membrane impedance were obtained through both simulation and analytical techniques (see *Eq. 4* and APPENDIX C). While an increase in temperature entailed only moderate changes to the variance of the total membrane noise current, it redistributed the noise power in the current spectrum to higher frequencies (Fig. 7*A*). However, the membrane impedance, which "translates" current noise to voltage noise, was much less affected by temperature and exhibited low-pass filter characteristics with virtually identical cutoff frequencies at both temperatures (Fig. 7*B*). Combining these two facts yielded the explanation for the reduction of neuronal noise at warmer temperatures: The additional power at high frequencies of the current noise was not translated to voltage fluctuations, because the impedance values at these high frequencies were low (at both temperatures). In contrast, the reduction in low-frequency power of the current noise resulted in a lower contribution of these frequencies to voltage noise at the warm temperature so that overall voltage noise was reduced. Mathematically, the different behavior of total noise power and impedance cutoff in contrast to noise current cutoff can be understood from the formulas summarized in MATERIALS AND METHODS; for a derivation see APPENDIX C. From these expres-

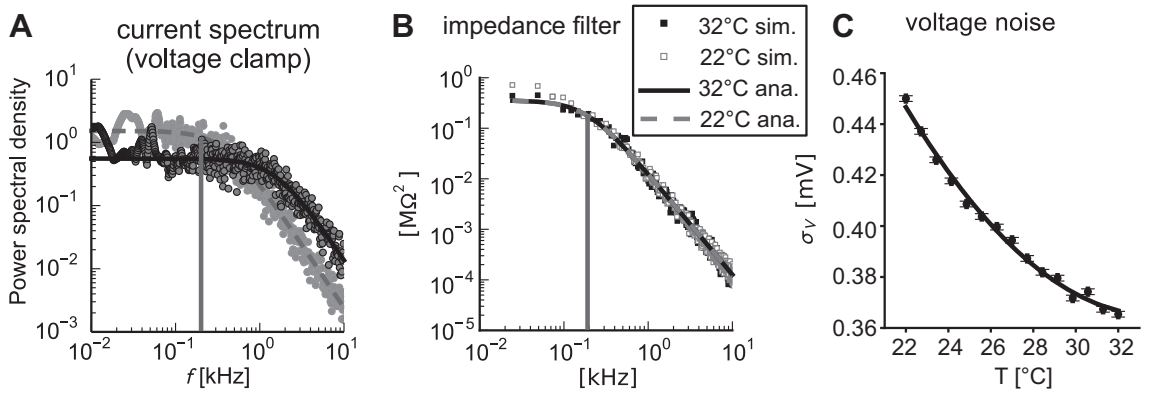

Fig. 7. *A*: power spectral density of the total current noise at 22°C (light gray, dashed line) and 32°C (dark gray, solid line) in voltage-clamp condition (command voltage is −67 mV). All stochastic ion channels, including the transduction, contribute to the fluctuations, but to different degrees. The weighted sum in *Eqs. 2* and *3* describes this behavior. Dots show estimated spectra, while lines are the theoretical prediction from *Eq. 4*. The main effect of the temperature increase is a shift of noise power to the high frequency range. Vertical line denotes the cutoff frequency of the impedance filter. *B*: temperature dependence of the membrane impedance filter in the subthreshold dynamical regime. Simulations (dots) are compared with the approximative, analytical formula (lines, *Eq. 6*). *C*: membrane voltage fluctuations near the resting state are reduced in the model neuron with higher temperature. The observed temperature dependence is a combination of the redistribution in noise power toward higher frequencies in *A* and the relative temperature invariance of the cutoff frequency of the membrane impedance in *B*. Parameters as in Fig. A2.

sions it is clear that only the noise cutoff frequency, $1/\tilde{\tau}(v,T)$, is influenced by the strong temperature susceptibilities of the reaction kinetics. In contrast, the total noise strength, i.e., the integral of the power spectrum, and membrane impedance depend on the Q_{10} values of the peak conductances only (APPENDIX B, *Eqs. 2* and *3*). The stronger temperature dependence of the cutoff frequency is a direct consequence of the fact that kinetic Q_{10} values are usually larger than the Q_{10} values of peak conductances. While the former Q_{10}s are found to be around 2.5–4 (Hille 2001), the latter lie close to the Q_{10} of aquatic diffusion coefficients, i.e., $\ll 2$.

DISCUSSION

The most remarkable finding of this study is a decrease of the overall trial-to-trial variability of auditory neuron responses at higher temperatures (Figs. 3 and 5). Several other response characteristics important for neuronal signaling were influenced by temperature in a similar way as reported for other auditory neurons; for example, action potential width and spike latencies decreased with rising temperature (Figs. 1 and 2; compare with Abrams and Pearson 1982; Coro et al. 1994; Fonseca and Correia 2007; Korsunovskaya and Zhantiev 2007). In view of the strong temperature influence on ion channels kinetics ($Q_{10} \sim 2.5$–4; Hille 2001), the observed decrease in spike jitter at first glance seemed counterintuitive.

Mathematical modeling explains effect of temperature on noise. We searched for a mechanistic explanation of the observed variability reduction by studying voltage fluctuations near threshold in a model introduced by Fisch et al. (2012). We demonstrated that increasing temperature redistributes current noise power to higher frequencies, which then are filtered out by the membrane impedance and hence contribute little to voltage variance (Fig. 7). Together this explains the voltage noise reduction at warmer temperatures. The change in the spectrum of the total noise current is also in accordance with the formulas given for single-channel noise spectra (DeFelice 1981; O'Donnell and van Rossum 2014). Our analytical treatment revealed under which conditions of the ion channels' Q_{10} parameters the reduction in voltage noise found in the simulations will take place. The total current noise power as well as the impedance cutoff are affected by the typically small Q_{10} values of peak conductances, while the cutoff frequency of the noise spectrum depends on the much larger Q_{10} values of opening and closing reaction rates (Hille 2001) and consequently show a stronger increase with temperature. On the basis of numerical simulations voltage fluctuations near threshold have previously been described in conductance-based models, where a qualitatively similar trend for temperature change was observed (Steinmetz et al. 2000).

In addition, the model was stimulated with the naturalistic songs used in the measurements. The experimentally observed reduction in trial-to-trial variability was reproduced by the model. We hence established that the model not only complies with the experimental spike statistics in a constant-stimulus paradigm at a single temperature (Fisch et al. 2012) but also agrees with data for naturalistic time-dependent song stimuli at different temperatures. Our analytic formulae can be applied to models containing arbitrary ion channel combinations, in order to analyze their impact on the noise statistics. In future work, this will enable the detection of compensatory mechanisms between the large amount of existing ion channels with their different timescales and temperature susceptibilities. While it has been demonstrated experimentally that ion channels, such as K_v1 potassium channels, have an impact on cortical spike variability (Higgs and Spain 2011), our quantitative understanding of how the potpourri of channels present in nerve membranes jointly impact the voltage fluctuations is still incomplete. The mathematical ansatz in APPENDIX C can support a more rigorous analysis in this direction.

Relevance of temperature and noise. The body temperature of grasshoppers is tightly coupled to the ambient temperature, and their body functions have to be maintained over a broad temperature range of >20°C. In particular, the neuronal processing of calling and courtship songs is crucial for the recognition and attraction of sexual partners and is strongly influenced by temperature (Bauer and von Helversen 1987; Ronacher and Stange 2013; von Helversen 1972, von Helversen 1979). The songs of many grasshopper species com-

prise fast amplitude modulations that constitute important signals for species recognition and sexual selection (Elsner 1974; Kriegbaum 1989; Ronacher and Römer 1985; Ronacher and Stumpner 1988; von Helversen 1979). Hence, elements of the auditory pathway should attain a high temporal resolution to allow for a robust evaluation of sexual signals—and spike train variability is detrimental for this task (Neuhofer et al. 2011; Ronacher 2014).

Grasshopper auditory receptor neurons encode the fine structure of amplitude modulations of sound stimuli in their instantaneous firing rate (Machens et al. 2001; Wohlgemuth et al. 2011). The lower intrinsic variability at warmer temperatures hence could allow for a better resolution of fine temporal details. This is supported by studies using a modulation transfer function paradigm that demonstrated an increased temporal resolution of auditory receptor neurons at higher temperature (Franz and Ronacher 2002; Prinz and Ronacher 2002; Ronacher and Römer 1985). Indeed, grasshoppers tested in a behavioral gap detection paradigm were able to detect gaps as small as 2 ms at 30°C, whereas at 22°C the minimal detected gap width was ~4 ms (Ronacher and Stumpner 1988). Similar improvements of temporal resolution with increasing temperature have been found in the fly's visual system (Tatler et al. 2000; Warzecha et al. 1999).

In summary, an elevated temperature leads to a reduction of spike timing variability in the grasshopper auditory periphery, which can be explained by a net decrease in the impact of channel noise on membrane voltage. The mechanisms, characterized in the mathematical model, are likely to generalize and to apply to neurons beyond the specific system at hand. This study shows that in order to decipher the effect of temperature on neuronal computation and to understand principles that enable a robustness to temperature changes (Caplan 2014; Rinberg et al. 2013; Robertson and Money 2012; Roemschied et al. 2014), not only deterministic but also stochastic mechanisms need to be taken into account. Further studies must reveal how the interplay of several different temperature-mediated effects leads to the robust encoding of auditory signals, which is reflected in the behavior of grasshoppers that respond to acoustic signals within a large temperature range.

APPENDIX A: NORMALIZATION OF THE VAN ROSSUM METRIC

The original van Rossum metric (van Rossum 2001) is defined by $\tilde{d}^2 = \int([y_1(t) - y_2(t)] * h(t))^2 \mathrm{d}t$, in which two Dirac-spike trains are denoted as $y_{1,2}(t) = \sum_{k=1}^{N_{sp}^{(1,2)}} \delta(t - t_k^{(1,2)})$, with spikes occurring at times $t_k^{(1)}$ and $t_k^{(2)}$. The convolution operator is denoted by *, and $h(t)$ is either an exponential kernel, $h(t) = H(t)\sqrt{2/\tau}e^{-t/\tau}$ (van Rossum 2001), or the synaptic α-function (Machens et al. 2003). H denotes Heaviside's step function: $H(t) = 1$ if $t > 0$ and $H(t) = 0$ if $t < 0$.

In the main text, a normalized version of the van Rossum metric is used. The square of the original expression is divided by the spike count, N_{sp}, to obtain

$$d^2 = \frac{2\tilde{d}^2}{N_{sp}^{(1)} + N_{sp}^{(2)}} = \frac{2}{N_{sp}^{(1)} + N_{sp}^{(2)}} \int \left([y_1(t) - y_2(t)] * h(t)\right)^2 \mathrm{d}t$$

The motivation for the normalization is to obtain a measure by which cold and hot spike train variabilities can be put into perspective, even if the spike counts are different. Figure A1 shows that the unnormalized van Rossum distance $\tilde{d}$ between two Poisson processes, indeed, scales with the square root of the mean spike count. The figure shows an example with $\tau = 2$, but note that the graph is independent of the timescale τ. The same scaling is found for two inhomogeneous Poisson processes with the same instantaneous rates and, generically, for all Poisson processes in the limit of small τ (Tomas and Sousa 2008).

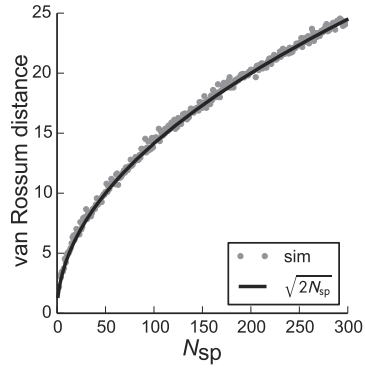

Fig. A1. Unnormalized spike train metric, $\tilde{d}$, for 2 independent Poisson processes with increasing number of spikes. Solid line shows the theoretical square-root scaling of the spike metric, and dots are simulated Poisson processes. N_{sp}, spike count.

APPENDIX B: AUDITORY RECEPTOR MODEL

The current balance equation for the voltage, $v(t)$, of a single-compartment model of the auditory receptors in locusts, proposed in Fisch et al. (2012), reads

$$c\dot{v} + I_{Na} + I_K + I_L + I_M + I_R = 0$$

It comprises the ionic currents I_{Na}, I_K, and I_L, responsible for the spike generation, as well as an M-type adaptation current, I_M, and the receptors' transduction current, I_R. The membrane capacitance c is 1 μF/cm^2. All parameter values can be found in Table 4.

The tympanal deflections, $x(t)$, induced by an external sound pressure wave, $s(t) = 20 \times 10^{I_{db}(t)}/20\xi_s(t)$, are described as a damped stochastic oscillation

$$\ddot{x} + (2/\tau_d)\dot{x} + \omega_{ty}{}^2 x = \alpha s(t) + \sigma_{ty}\xi_x(t) \quad (7)$$

The input s(t) is imbibed with a gain factor α, which was determined from stroboscopic measurements (Breckow and Sippel 1985; Fisch et al. 2012). The thermal fluctuations ξ_x of the tympanum are a white noise process with variance $\sigma_{ty}^2 = (4\alpha k_B T)/(\tau_d B)$, where B is the vibrating area of the tympanum and k_B is Bolzmann's constant. The eigenfrequency and the damping time constant of the tympanum, ω_{ty} and τ_d, respectively, have previously been determined by laser vibrometry (Eberhard et al. 2014; Schiolten et al. 1981).

The tympanal vibrations are transduced into a receptor current $I_R = G_R(t)(v - E_R)$ by an unidentified receptor, possibly of the TRP family as in *Drosophila* (Zhang et al. 2013). The receptor channel is assumed to have two states, follows first-order kinetics, and has an activation function described by Howard and Hudspeth (1988) and Hudspeth et al. (2000)

$$z_\infty(x) = \frac{1}{1 + \exp\left(-\frac{k_s}{k_B T}(x - x_{base})\right)} + \frac{1}{1 + \exp\left(\frac{k_s}{k_B T}(x + x_{base})\right)}$$

The spring constant k_s, the half-maximum of the mechano-transducer x_{base}, and the tympanal gain α were adapted to fit the recorded rate-intensity curves (cf. Fig. 6*B*). All other channels follow typical Markov state models from the literature (Fisch et al. 2012).

In total, there are three different noise sources in the equations above: first of all, thermal noise from the tympanum (ξ_x); second, the

Table 4. *Model parameters*

Parameter	Value	Parameter	Value
N_M	600	τ_h, ms	$\frac{(e^{-\frac{v}{5}-\frac{27}{5}}+1)}{0.128(e^{-\frac{v}{5}-\frac{27}{5}}+1)e^{-\frac{v}{18}-\frac{25}{9}}+4}$ ms
N_K	40,000		
N_R	10		
N_{Na}	40,000		
k_B	13.8 μm^2 fg/(ms^2 K)	τ_n, ms	$\frac{(-e^{-\frac{v}{5}-\frac{52}{5}}+1)}{0.032v-0.5(e^{-\frac{v}{5}-\frac{52}{5}}-1)e^{-\frac{v}{40}-\frac{57}{40}}+1.664}$ ms
x_{base}	0.26 μm		
g_K	80 mS/cm^2		
g_R	0.5 mS/cm^2		
g_{Na}	100 mS/cm^2	τ_m, ms	$\frac{(e^{-\frac{v}{4}-\frac{27}{2}}-1)(e^{\frac{v}{5}+\frac{27}{5}}-1)}{(0.28v+7.56)(e^{-\frac{v}{4}-\frac{27}{2}}-1)-(0.32v+17.28)(e^{\frac{v}{5}+\frac{27}{5}}-1)}$ ms
g_M	5 mS/cm^2		
g_L	0.15 mS/cm^2		
E_M	−100 mV		
E_L	−67 mV	h_∞	$\frac{0.128(e^{-\frac{v}{5}-\frac{27}{5}}+1)e^{-\frac{v}{18}-\frac{25}{9}}}{(0.128)(e^{-\frac{v}{5}-\frac{27}{5}}+1)e^{-\frac{v}{18}-\frac{25}{9}}+4}$
E_K	−100 mV		
E_{Na}	50 mV		
B	1 mm^2		
E_R	0 mV	w_∞	$\frac{1}{e^{-\frac{v}{5}-4}+1}$
a	0.003 μm^2/fg		
c	1 μF/cm^2		
T_{base}	295.15 K	m_∞	$-\frac{(0.32v+17.28)(e^{\frac{v}{5}+\frac{27}{5}}-1)}{(0.28v+7.56)(e^{-\frac{v}{4}-\frac{27}{2}}-1)-(0.32v+17.28)(e^{\frac{v}{5}+\frac{25}{5}}-1)}$
w_{tymp}	25.13 kHz		
k_s	91,826.75 μm fg/ms^2		
τ_d	0.1 ms	n_∞	$\frac{0.032v+1.664}{0.032v-0.5(e^{-\frac{v}{5}-\frac{52}{5}}-1)e^{-\frac{v}{40}-\frac{57}{40}}+1.664}$
τ_z	1.19 ms		
τ_w	100 ms		

input, which consists of a modulated white noise carrier (ξ_s); and third, noise from stochastic ion channel gating, discussed next.

Stochastic ion channels. Instead of simulating the master equations for the stochastic ion channels, one (Linaro et al. 2011) of several (Fox and Lu 1994; Goldwyn et al. 2011; Orio and Soudry 2012) diffusion approximations available in the literature are used. This casts the problem into a stochastic differential equation (SDE), which facilitates the following mathematical analysis.

As an example, take the receptor channel from above. It is modeled as a two-state (open-closed) Markov model (Fisch et al. 2012). The gating variable G_R that approximates the two-state Markov dynamics can be split into a deterministic z and a stochastic η_z part, $G_R = \bar{g}_R(z + \eta_z)$. According to Linaro et al. (2011) the governing equations read

$$\begin{aligned} \tau_z(T)\dot{z} &= \big(z_\infty(x) - z\big), \\ \tau_z(T)\dot{\eta}_z &= -\eta_z + \sqrt{2\tau_z}\sigma_z\xi_z(t) \end{aligned} \tag{8}$$

In the two-state case, the noise variance given by Fox and Lu (1994) is valid. It reads $\sigma_z^2 = \tau_z(z_\infty(x)(1 - z) + (1 - z_\infty(x))z)$, which in the steady state becomes

$$\sigma_z^2(x) = {N_R}^{-1} z_\infty(x)\big(1 - z_\infty(x)\big)$$

For fixed tympanal position x, *Eq. 8* is an Ornstein-Uhlenbeck (OU) process. The temperature dependence of $\tau_z(T)$ follows *Eq. 1*.

Ion channels with $n > 2$-dimensional state space require as many OU processes to represent the correlation structure as there are reactions. The voltage-dependent activation curves and time constants of these OU processes are obtained from an eigendecomposition of the infinitesimal transition matrices of the Markov models (Tuckwell 1989). For the Na^+ and K^+ channels used here, they are given in Linaro et al. (2011). The M-type adaptation conductance is modeled as a two-state channel like the receptor.

APPENDIX C: MODEL ANALYSIS

The complete rate-intensity curve of a nonlinear and stochastic membrane is not analytically tractable. The calculation of the statistical properties of the firing rate can be divided into three mathematical problems: *1*) well below threshold, the firing rate is given as an escape process, with Poisson statistics; *2*) well above threshold, the system exhibits a stochastic limit cycle, with inverse Gaussian statistics; *3*) an intermediate regime where both descriptions break. The intermediate regime is important for amplitude coding, as it spans the largest dynamic range. The spike fluctuations in that regime are related to voltage noise (O'Donnell and van Rossum 2014). Hence, the following calculation focuses on deriving the voltage noise close to threshold under varying temperature.

Simplification of the transduction. To start with, the transduction dynamics is simplified. This step reduces the simulation time, because the integration of the tympanal oscillations of the full system would render the SDE system stiff. Furthermore, the transduction channel can now be treated as just one more channel that contributes to the total voltage noise.

Note from the model parameters in Table 4 that the difference in timescale between the eigenfrequency of the tympanum and the time constant of the receptor channel, $\tau_z > 2\pi/\omega_{ty}$, prevents a locking of spikes to the tympanal oscillations, in accordance with experimental observations (Sippel and Breckow 1983). Moreover, this difference in timescale allows for an adiabatic elimination (Titulaer 1980) of the fast variables x and $\dot{x}$, leaving us with analytic expressions for mean and variance of the receptor gating variable, z, as a function of the input intensity I_{db}. This procedure formalizes the intuition that because the receptor kinetics are slower than the tympanal dynamics, they are only affected by the average statistics of the deflections. Thus it suffices to take the equilibrium distribution, $p_\infty(x; I_{db})$, of the tympanum's vibrations to average over *Eq. 8*. Since *Eq. 7* is a noisy harmonic oscillator, the marginal equilibrium distribution of the tympanal excursion, x, is given by

$$p_\infty(x; I_{db}) = \left(\sqrt{2\pi}\sigma_x\right)^{-1}\exp\left(-\frac{x^2}{2\sigma_x^2}\right) \tag{9}$$

The dependence on the input I_{db} is mediated by the variance

$$\sigma_x^2 = \left(\left(\alpha \cdot 20 \times 10^{I_{db}/20}\right)^2 + {\sigma_{ty}}^2\right)\tau_d/4{\omega_{ty}}^2$$

i.e., a louder sound produces a larger deviation in the tympanal deflections. The theoretical distributions and the histograms obtained from numerical simulations at two input intensities are illustrated in Fig. A2*A*.

Applying the adiabatic elimination procedure (Titulaer 1980) to the drift and diffusion parts of *Eq. 8* requires calculation of the averaged steady-state activation curve

$$\tilde{z}_\infty(I_{db}) = \int_{-\infty}^{\infty} dx\, p_\infty(x;I_{db}) z_\infty(x) \approx 1 - \frac{\tanh\left(k_S x_{base}/\left(2k_B T\right)\right)}{\left(1 + \left(\frac{k_S \sigma_X}{k_B T}\mathrm{sech}\left(\frac{k_S x_{base}}{2k_B T}\right)\right)^2\right)^{\frac{1}{2}}} \quad (10)$$

To obtain the analytical approximations above, the activation function z_∞ is approximated by a Gaussian, so that the integrals can be evaluated using Laplace's method (MacKay 2003).

In addition, the averaged diffusion coefficient is needed. So, *mutatis mutandis*, $z_\infty(1 - z_\infty)$ can be approximated by 1 minus a Gaussian, which yields

$$\tilde{\sigma}_z^2(I_{db}) = \int_{-\infty}^{\infty} dx\, p_\infty(x;I_{db})\sigma_z^2(x) \approx \frac{\frac{\beta {x_{base}}^2}{2e^{2\left(1-\beta\sigma_x^2\right)}}\left(\frac{1}{4} - \frac{1}{\left(1 + e^{2k_S x_{base}/k_B T}\right)^2}\right)}{N_R\sqrt{1-\beta\sigma_x^2}} \quad (11)$$

where

$$\beta = -\frac{k_s^2\left(5 + 40e^{2k_s x_{base}/k_B T} + 18e^{4k_s x_{base}/k_B T} + e^{8k_s x_{base}/k_B T}\right)}{2\left(3 + 4e^{2k_s x_{base}/k_B T} + e^{4k_s x_{base}/k_B T}\right)^2 k_B^2 T^2}$$

The reduced gating SDE for the two-state receptor channel then has the following structure

$$\tau_z(T)\dot{z} = z_\infty(I_{db}) - z + \sqrt{2\tau_z}\sigma_z(I_{db})\xi_z(t)$$

The symbol $\xi_z(t)$ denotes a zero-mean, white noise process. In this approximation, for any fixed mean input I_{db} and temperature T, the transduction gating variable will be Gaussian. This effectively eliminates the state space dimensions corresponding to the noisy tympanal oscillations. The accuracy of this approximation can be inspected in Fig. A2, *B* and *C*.

Noise current spectrum. The currents in the balance equation for the voltage dynamics can be separated into deterministic, $I_d(v)$, and stochastic, $I_f(v)$, parts

$$C\dot{v} + I_d(v) + I_f(v) = 0$$

The drift contains the deterministic model components. Near the fixed point it reads

$$I_d(v) = \bar{g}_{Na}(T)m_\infty^3(v)h_\infty(v)\left(v - E_{Na}(T)\right) + \bar{g}_K(T)n_\infty^4(v)\left(v - E_K(T)\right) + \bar{g}_L(T)\left(v - E_L(T)\right) + \bar{g}_M(T)w\left(v - E_M(T)\right) + \bar{g}_R(T)\tilde{z}_\infty(I_{db})\left(v - E_R(T)\right)$$

while the stochastic part is

$$I_f(v) = \bar{g}_{Na}(T)\left(v - E_{Na}(T)\right)\sum_{k=1}^{M_{Na}-1}\eta_k + \bar{g}_K(T)\left(v - E_K(T)\right)\sum_{j=1}^{M_K-1}\eta_j + \bar{g}_M(T)\left(v - E_M(T)\right)\eta_w + \bar{g}_R(T)\left(v - E_R(T)\right)\eta_z$$

Here, M_c is the number of states of the $c \in \{Na,K,M,R\}$-channel. The noise processes are exponentially correlated OU processes

$$\tau_k(v,T)\dot{\eta}_k = -\eta_k + \sqrt{2\tau_k(v,T)}\sigma_k(v)\xi_k$$

where all ξ_ks denote zero-mean, white noise processes. The analytic expressions for the voltage-dependent variances $\sigma_k(v)$ and time constants $\tau_k(v,T)$ are determined from the eigenvectors and eigenvalues of the infinitesimal transition matrix of the Markov chains, respectively (Linaro et al. 2011; Tuckwell 1989). The expression for the variance of the receptor channel was derived in *Eq. 11*.

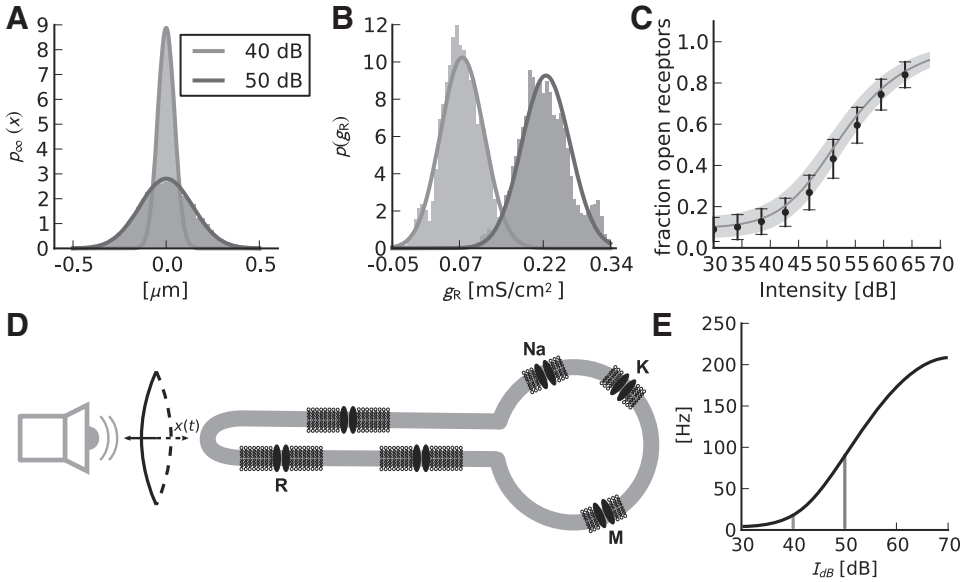

Fig. A2. Comparison between theory and simulation for the receptor model with transduction. *A*: probability distribution of tympanal deflections (as indicated in the schematic in *D*) in response to white noise stimuli at 2 different sound intensities (I_{db} = 40 dB SPL and I_{db} = 50 dB SPL). Solid lines represent the Gaussian distribution from *Eq. 9*. *B*: probability distributions of the conductance fluctuations of the receptor channels (depicted in *D*, R) induced by the 2 inputs. Solid lines represent theoretical predictions based on the quasi-static averaging, *Eqs. 10* and *11*. *C*: comparison of the mean and variance of the receptor gate z as a function of the sound input. Black dots depict the mean open probability, and error bars denote the standard deviation. The dark gray line shows the theoretical curve from *Eq. 10*, and the gray shaded area the standard deviation, see *Eq. 11*. *E*: sketch of the rate-intensity curve. The intensity and fluctuations of the transduction current are translated into a spike frequency by voltage-dependent ion channels (depicted in *D*), resulting in a rate-intensity curve. The 2 output frequencies for I_{db} = 40, 50 dB are marked by vertical lines. T = 22°C, all other parameters as given in Tables 3 and 4.

As a next step, the fluctuating part is approximated by a single OU process, fitted to reproduce the correlation time of the superposition of OU processes in I_f. The autocorrelation of I_f under voltage clamp and in steady state is

$$\langle I_f(t) I_f(t+\Delta)\rangle = \bar{g}_{Na}{}^2 (v - E_{Na})^2 \sum_{k=1}^{M_{Na}-1} \sigma_k{}^2(v) e^{-\|\Delta\|/\tau_k(v)} + \bar{g}_K (v - E_K)^2 \sum_{j=1}^{M_K-1} \sigma_j(v)^2 e^{-\|\Delta\|/\tau_j(v)} + \bar{g}_M{}^2 (v - E_K)^2 \sigma_M(v)^2 e^{-\|\Delta\|/\tau_M(v)} + \bar{g}_R{}^2 (v - E_K)^2 \bar{\sigma}_R^2 (I_{db}) e^{-\|\Delta\|/\tau_z}$$

This is approximated by a single OU process, $\breve{\eta}$ with correlation $\breve{\sigma}^2(v,T) e^{-\|\Delta\|/\breve{\tau}(v,T)}$, by Taylor expanding both the single OU and the sum of OUs. Based on this expression both σ and τ can be identifed (see *Eqs. 2* and *3*).

Hence, the power spectrum of the total noise current is the Fourier transform of the correlation function at a clamped command voltage v is then approximately a Lorentzian

$$P_i(f) = \frac{\breve{\tau}(v)\breve{\sigma}^2(v)}{1 + (f\breve{\tau}(v))^2}.$$

Importantly, the total variance of the membrane current, σ^2, is only affected by the Q_{10} values of the peak conductances, which are relatively small (<2.0). On the other hand, the cutoff frequency, $\breve{t}^{-1}$, of the total membrane noise current depends on the Q_{10} parameters of reaction kinetics, which are comparatively large (>2.0). This leads to the redistribution of noise power to higher frequencies shown in Fig. 7*A*.

Membrane impedance. The subthreshold impedance filter can be derived by linearization around the resting potential. The poles and zeros of the impedance filter are then related to the eigenvalues of the system's Jacobian matrix. In the case of a type 1 neuron this simplifies and the impedance is a low-pass filter approximately given by

$$Z(f) \approx \frac{1}{\left(\left(\frac{1}{c}\frac{\partial I_f}{\partial V}\right)^2 + f^2\right)}$$

Note that the steady-state value of $\partial I_f/\partial V$ only depends on the Q_{10} parameters of the peak conductances. Consequently, the impedance is affected by temperature to a lesser degree, as can be seen in Fig. 7*B*.

Together with the conclusion of the previous section this means: If all $Q_{10}(g_c)$ values are well below 2 and the $Q_{10}(\tau_i)$ values are sufficiently large, voltage noise fluctuations are reduced when temperature increases (cf. Fig. 7*C*).

ACKNOWLEDGMENTS

We thank J. Clemens for providing help to M. J. B. Eberhard concerning MATLAB programming and F. Roemschied for providing a tool to calculate mean action potential shape.

GRANTS

This work was funded by the German Research Council (DFG: SFB 618, grant to B. Ronacher and S. Schreiber, RO547/12-1) and the Federal Ministry of Education and Research, Germany (01GQ1001A, 01GQ0901, 01GQ0972, grants to B. Ronacher and S. Schreiber).

DISCLOSURES

No conflicts of interest, financial or otherwise, are declared by the author(s).

AUTHOR CONTRIBUTIONS

Author contributions: M.J.B.E., J.-H.S., and B.R. conception and design of research; M.J.B.E. and J.-H.S. performed experiments; M.J.B.E. and J.-H.S. analyzed data; M.J.B.E., J.-H.S., S.S., and B.R. interpreted results of experiments; M.J.B.E. and J.-H.S. prepared figures; M.J.B.E., J.-H.S., and B.R. drafted manuscript; M.J.B.E., J.-H.S., S.S., and B.R. edited and revised manuscript; M.J.B.E., J.-H.S., S.S., and B.R. approved final version of manuscript.

REFERENCES

Abrams TW, Pearson KG. Effects of temperature on identified central neurons that control jumping in the grasshopper. *J Neurosci* 2: 1538–1553, 1982.

Alijani AK, Richardson MJ. Rate response of neurons subject to fast or frozen noise: from stochastic and homogeneous to deterministic and heterogeneous populations. *Phys Rev E Stat Nonlin Soft Matter Phys* 84: 011919, 2011.

Bauer M, von Helversen O. Separate localization of sound recognizing and sound producing neural mechanisms in a grasshopper. *J Comp Physiol A* 161: 95–101, 1987.

Breckow J, Sippel M. Mechanics of the transduction of sound in the tympanal organ of adults and larvae of locusts. *J Comp Physiol A* 157: 619–629, 1985.

Burrows M. Effects of temperature on a central synapse between identified motor neurons in the locust. *J Comp Physiol A* 165: 687–695, 1989.

Caplan JS, Williams AH, Marder E. Many parameter sets in a multicompartment model oscillator are robust to temperature perturbations. *J Neurosci* 34: 4963–4975, 2014.

Clemens J, Wohlgemuth S, Ronacher B. Nonlinear computations underlying temporal and population sparseness in the auditory system of the grasshopper. *J Neurosci* 32: 10053–10062, 2012.

Coro F, Pérez M, Machado A. Effects of temperature on a moth auditory receptor. *J Comp Physiol A* 174: 517–525, 1994.

DeFelice LJ. *Introduction to Membrane Noise*. New York: Plenum, 1981.

Eberhard MB, Gordon S, Windmill JC, Ronacher B. Temperature effects on the tympanal membrane and auditory receptor neurons in the locust. *J Comp Physiol A Neuroethol Sens Neural Behav Physiol* 200: 837–847, 2014.

Elsner N. Neuroethology of sound production in gomphocerine grasshoppers (Orthoptera: Acrididae). *J Comp Physiol* 88: 67–102, 1974.

Fisch K, Schwalger T, Lindner B, Herz AV, Benda J. Channel noise from both slow adaptation currents and fast currents is required to explain spike-response variability in a sensory neuron. *J Neurosci* 32: 17332–17344, 2012.

Fonseca PJ, Correia T. Effects of temperature on tuning of the auditory pathway in the cicada *Tettigetta josei* (Hemiptera, Tibicinidae). *J Exp Biol* 210: 1834–1845, 2007.

Fortin FA, De Rainville FM, Gardner MA, Parizeau M, Gagné C. DEAP: evolutionary algorithms made easy. *J Mach Learn Res* 13: 2171–2175, 2012.

Fox RF, Lu Yn. Emergent collective behavior in large numbers of globally coupled independently stochastic ion channels. *Phys Rev E Stat Phys Plasmas Fluids Relat Interdiscip Topics* 49: 3421–3431, 1994.

Franz AF, Ronacher BR. Temperature dependence of temporal resolution in an insect nervous system. *J Comp Physiol A* 188: 261–271, 2002.

Goldwyn JH, Imennov NS, Famulare M, Shea-Brown E. Stochastic differential equation models for ion channel noise in Hodgkin-Huxley neurons. *Phys Rev E Stat Nonlin Soft Matter Phys* 83: 041908, 2011.

Higgs MH, Spain WJ. Kv1 channels control spike threshold dynamics and spike timing in cortical pyramidal neurones. *J Physiol* 589: 5125–5142, 2011.

Hille B. *Ionic Channels of Excitable Membranes*. Sunderland, MA: Sinauer, 2001.

Hoffmann KH. Stoffwechsel. In: *Physiologie der Insekten*, edited by Gewecke M. Stuttgart, Germany: Fischer, 1995, p. 1–65.

Howard J, Hudspeth A. Compliance of the hair bundle associated with gating of mechanoelectrical transduction channels in the bullfrog's saccular hair cell. *Neuron* 1: 189–199, 1988.

Hudspeth AJ, Choe Y, Mehta AD, Martin P. Putting ion channels to work: mechanoelectrical transduction, adaptation, and amplification by hair cells. *Proc Natl Acad Sci USA* 97: 11765–11772, 2000.

Janssen R. Thermal influences on nervous system function. *Neurosci Biobehav Rev* 16: 399–413, 1992.

Korsunovskaya O, Zhantiev R. Effect of temperature on auditory receptor functions in crickets (Orthoptera, Tettigoniodea). *J Evol Biochem Phys* 43: 327–334, 2007.

Kriegbaum H. Female choice in the grasshopper *Chorthippus biguttulus*. *Naturwissenschaften* 76: 81–82, 1989.

Linaro D, Storace M, Giugliano M. Accurate and fast simulation of channel noise in conductance-based model neurons by diffusion approximation. *PLoS Comput Biol* 7: e1001102, 2011.

Machens CK, Schütze H, Franz A, Kolesnikova O, Stemmler MB, Ronacher B, Herz AV. Single auditory neurons rapidly discriminate conspecific communication signals. *Nat Neurosci* 6: 341–342, 2003.

Machens CK, Stemmler MB, Prinz P, Krahe R, Ronacher B, Herz AV. Representation of acoustic communication signals by insect auditory receptor neurons. *J Neurosci* 21: 3215–3227, 2001.

MacKay DJ. *Information Theory, Inference, and Learning Algorithms*. http://citeseerx.ist.psu.edu/viewdoc/download?doi=10.1.1.228.899&rep=rep1&type=pdf [17 Feb. 2015]

Montgomery JC, MacDonald JA. Effects of temperature on nervous system: implications for behavioral performance. *Am J Physiol Regul Integr Comp Physiol* 259: R191–R196, 1990.

Neuhofer D, Stemmler M, Ronacher B. Neuronal precision and the limits for acoustic signal recognition in a small neuronal network. *J Comp Physiol A Neuroethol Sens Neural Behav Physiol* 197: 251–265, 2011.

Neuhofer D, Wohlgemuth S, Stumpner A, Ronacher B. Evolutionarily conserved coding properties of auditory neurons across grasshopper species. *Proc R Soc Lond B Biol Sci* 275: 1965–1974, 2008.

O'Donnell C, van Rossum MC. Systematic analysis of the contributions of stochastic voltage gated channels to neuronal noise. *Front Comput Neurosci* 8: 105, 2014.

Orio P, Soudry D. Simple, fast and accurate implementation of the diffusion approximation algorithm for stochastic ion channels with multiple states. *PLoS One* 7: e36670, 2012.

Pearson KG, Robertson RM. Interneurons coactivating hindleg flexor and extensor motoneurons in the locust. *J Comp Physiol A* 144: 391–400, 1981.

Prinz PP, Ronacher BR. Temporal modulation transfer functions in auditory receptor fibres of the locust (*Locusta migratoria* L.). *J Comp Physiol A Neuroethol Sens Neural Behav Physiol* 188: 577–587, 2002.

Rinberg A, Taylor AL, Marder E. The effects of temperature on the stability of a neuronal oscillator. *PLoS Comput Biol* 9: e1002857, 2013.

Robertson RM, Money TG. Temperature and neuronal circuit function: compensation, tuning and tolerance. *Curr Opin Neurobiol* 22: 724–734, 2012.

Roemschied FA, Eberhard MJ, Schleimer JH, Ronacher B, Schreiber S. Cell-intrinsic mechanisms of temperature compensation in a grasshopper sensory receptor neuron. *eLife* 3: e02078, 2014.

Römer H, Marquart V. Morphology and physiology of auditory interneurons in the metathoracic ganglion of the locust. *J Comp Physiol A* 155: 249–262, 1984.

Ronacher B. Processing of species-specific signals in the auditory pathway of grasshoppers. In: *Insect Hearing and Acoustic Communication*, edited by Hedwig B. Berlin: Springer, 2014, p. 185–204.

Ronacher B, Römer H. Spike synchronization of tympanic receptor fibres in a grasshopper (*Chorthippus biguttulus* L., Acrididae). *J Comp Physiol A* 157: 631–642, 1985.

Ronacher B, Stange N. Processing of acoustic signals in grasshoppers—a neuroethological approach towards female choice. *J Physiol (Paris)* 107: 41–50, 2013.

Ronacher B, Stumpner A. Filtering of behaviourally relevant temporal parameters of a grasshopper's song by an auditory interneuron. *J Comp Physiol A* 163: 517–523, 1988.

Sanborn AF. Acoustic signals and temperature. In: *Insect Sounds and Communication*, edited by Drosopoulos S, Claridge MF. Boca Raton, FL: Taylor & Francis, 2006, p. 111–125.

Schiolten P, Larsen ON, Michelsen A. Mechanical time resolution in some insect ears. *J Comp Physiol* 143: 289–295, 1981.

Sippel M, Breckow J. Non-linear analysis of the transmission of signals in the auditory system of the migratory locust *Locusta migratoria*. *Biol Cybern* 46: 197–205, 1983.

Steinmetz PN, Manwani A, Koch C, London M, Segev I. Subthreshold voltage noise due to channel fluctuations in active neuronal membranes. *J Comput Neurosci* 9: 133–148, 2000.

Stimberg M, Goodman DF, Benichoux V, Brette R. Equation-oriented specification of neural models for simulations. *Front Neuroinform* 8: 6, 2014.

Stumpner A, Ronacher B. Auditory interneurones in the metathoracic ganglion of the grasshopper *Chorthippus biguttulus*. I. Morphological and physiological characterization. *J Exp Biol* 158: 391–410, 1991.

Stumpner A, Ronacher B, von Helversen O. Auditory interneurones in the metathoracic ganglion of the grasshopper *Chorthippus biguttulus*. II. Processing of temporal patterns of the song of the male. *J Exp Biol* 158: 411–430, 1991.

Tang LS, Goeritz ML, Caplan JS, Taylor AL, Fisek M, Marder E. Precise temperature compensation of phase in a rhythmic motor pattern. *PLoS Biol* 8: e1000469, 2010.

Tatler B, O'Carroll DC, Laughlin SB. Temperature and the temporal resolving power of fly photoreceptors. *J Comp Physiol A* 186: 399–407, 2000.

Titulaer UM. The Chapman-Enskog procedure as a form of degenerate perturbation theory. *Physica A* 100: 234–250, 1980.

Tomas P, Sousa L. Statistical analysis of a spike train distance in Poisson models. *IEEE Signal Process Lett* 15: 357–360, 2008.

Tuckwell HC. *Stochastic Processes in the Neurosciences*. Philadelphia, PA: Society for Industrial and Applied Mathematics, 1989.

van Rossum MC. A novel spike distance. *Neural Comput* 13: 751–763, 2001.

Vogel A, Ronacher B. Neural correlations increase between consecutive processing levels in the auditory system of locusts. *J Neurophysiol* 97: 3376–3385, 2007.

von Helversen D. Gesang des Männchens und Lautschema des Weibchens bei der Feldheuschrecke *Chorthippus biguttulus* (Orthoptera, Acrididae). *J Comp Physiol* 81: 381–422, 1972.

von Helversen D, von Helversen O. Recognition of sex in the acoustic communication of the grasshopper *Chorthippus biguttulus (Orthoptera, Acrididae)*. *J Comp Physiol A* 180: 373–386, 1997.

von Helversen O. Angeborenes Erkennen akustischer Schlüsselreize. *Verh Dtsch Zool Ges* 72: 42–59, 1979.

Warzecha A, Horstmann W, Egelhaaf M. Temperature-dependence of neuronal performance in the motion pathway of the blowfly *Calliphora erythrocephala*. *J Exp Biol* 202: 3161–3170, 1999.

Wohlgemuth S, Ronacher B. Auditory discrimination of amplitude modulations based on metric distances of spike trains. *J Neurophysiol* 97: 3082–3092, 2007.

Wohlgemuth S, Vogel A, Ronacher B. Encoding of amplitude modulations by auditory neurons of the locust: influence of modulation frequency, rise time, and modulation depth. *J Comp Physiol A Neuroethol Sens Neural Behav Physiol* 197: 61–74, 2011.

Zhang W, Yan Z, Jan LY, Jan YN. Sound response mediated by the TRP channels NOMPC, NANCHUNG, and INACTIVE in chordotonal organs of *Drosophila* larvae. *Proc Natl Acad Sci USA* 110: 13612–13617, 2013.